FULL PAPER

Relativistic electron flux growth during storm and non-storm periods as observed by ARASE and GOES satellites

Vladimir Borisovich Belakhovsky[1*] , Vyacheslav A. Pilipenko[2], Elizaveta E. Antonova[3], Yoshizumi Miyoshi[4], Yoshiya Kasahara[5], Satoshi Kasahara[6], Nana Higashio[7], Iku Shinohara[7,8], Tomoaki Hori[9], Shoya Matsuda[5], Shoichiro Yokota[10], Takeshi Takashima[7,8], Mitani Takefumi[7,8], Kunihiro Keika[6] and Satoko Nakamura[7,8]

Abstract

Variations of relativistic electron fluxes ($E \geq 1$ MeV) and wave activity in the Earth magnetosphere are studied to determine the contribution of different acceleration mechanisms of the outer radiation belt electrons: ULF mechanism, VLF mechanism, and adiabatic acceleration. The electron fluxes were measured by Arase satellite and geostationary GOES satellites. The ULF power index is used to characterize the magnetospheric wave activity in the Pc5 range. To characterize the VLF wave activity in the magnetosphere, we use data from PWE instrument of Arase satellite. We consider some of the most powerful magnetic storms during the Arase era: May 27–29, 2017; September 7–10, 2017; and August 25–28, 2018. Also, non-storm intervals with a high solar wind speed before and after these storms for comparison are analyzed. Magnitudes of relativistic electron fluxes during these magnetic storms are found to be greater than that during non-storm intervals with high solar wind streams. During magnetic storms, the flux intensity maximum shifts to lower L-shells compared to intervals without magnetic storms. For the considered events, the substorm activity, as characterized by AE index, is found to be a necessary condition for the increase of relativistic electron fluxes, whereas a high solar wind speed alone is not sufficient for the relativistic electron growth. The enhancement of relativistic electron fluxes by 1.5–2 orders of magnitude is observed 1–3 days after the growth of the ULF index and VLF emission power. The growth of VLF and ULF wave powers coincides with the growth of substorm activity and occurs approximately at the same time. Both mechanisms operate at the first phase of electron acceleration. At the second phase of electron acceleration, the mechanism associated with the injection of electrons into the region of the magnetic field weakened by the ring current and their subsequent betatron acceleration during the magnetic field restoration can work effectively.

Keywords Magnetosphere, Outer radiation belt, Relativistic electrons, Magnetic storm, Substorm, ULF waves, VLF waves
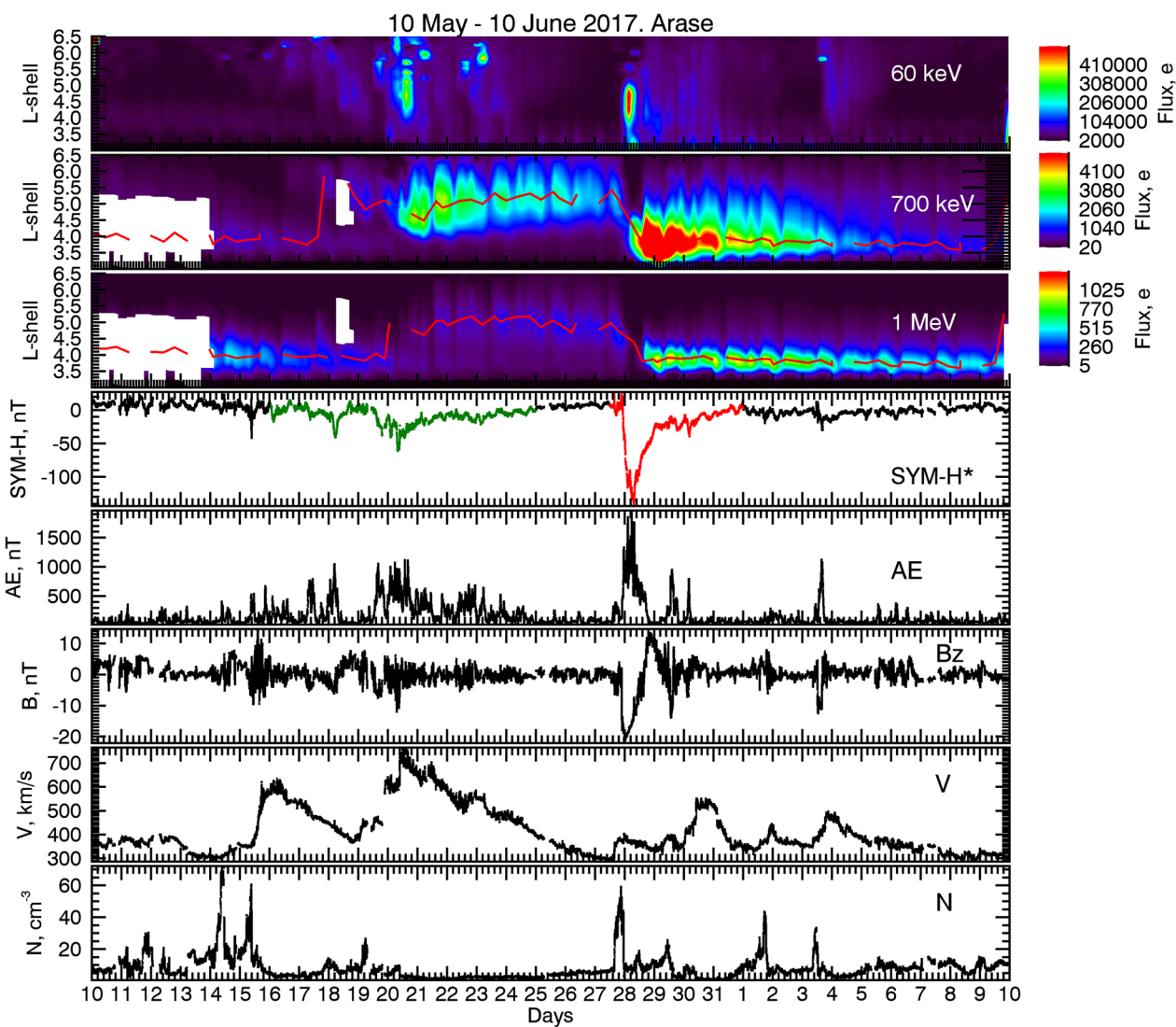
*Correspondence:
Vladimir Borisovich Belakhovsky
belakhov@mail.ru
Full list of author information is available at the end of the article

Belakhovsky *et al. Earth, Planets and Space*   (2023) 75:189

Page 2 of 17

Graphical Abstract

10 May – 10 June 2017. Arase

Introduction

The fluxes of relativistic electrons in the outer radiation belt (ORB) vary by several orders of magnitude, especially during periods of enhanced geomagnetic activity. Relativistic "killer" electrons can destroy the satellite electronic equipment and provide harmful radiation dose for astronauts (Pilipenko et al. 2006; Baker and Daglis 2007). Identification of mechanisms responsible for the magnetospheric electron energization to relativistic energies (≥1 MeV) is still a challenge for the space physics. While the electrodynamics of the near-Earth space is

driven by the solar wind and interplanetary magnetic field (IMF), the energization of magnetospheric electrons is caused by some inner-magnetospheric processes. In collisionless space plasma the solar wind flow does not interact directly with trapped magnetospheric electrons. Therefore, electromagnetic fields play a role of intermediary transferring the energy from low-energy particles to a small group of high-energy electrons. The problem of magnetosphere electron acceleration is challenging not only from a practical point of view, but because of fundamental reasons, as well. Indeed, during this process

Belakhovsky *et al. Earth, Planets and Space*   (2023) 75:189

Page 3 of 17

somehow energy is transferred from particles with a relatively low energy to particles with more than 5 orders of magnitude larger energies, which seemingly contradicts the principles of thermodynamics.

The relativistic electron enhancement is known to be closely associated with intense geomagnetic storms, in which intensity is characterized by Dst index (Baker and Daglis 2007). However, even moderate geomagnetic disturbances were found to lead to comparable and even greater growth of the relativistic electrons (Borovsky and Denton 2006; Schiller et al. 2014). Statistical studies demonstrated that not every geomagnetic storm produced relativistic electron flux enhancement at the geostationary orbit. For example, Reeves et al. (2003) analyzing LANL and Polar data showed that ~ 50% of storms exhibited a high-energy electron flux increase, while ~ 25% showed an actual flux decrease, and ~ 25% showed no flux change. Moya et al. (2017) based on Van Allen Probes data showed that enhancement events were common for ~2 MeV electrons at L~5, but their number decreased with increasing energy at any given L shell.

A good correlation between the growth of the relativistic electron fluxes (> 2 MeV), mainly at the geosynchronous orbit, and solar wind velocity were found (Paulikas and Blake 1979; Baker et al. 1979; Lyatsky and Khazanov 2008; Potapov et al. 2012). Besides the solar wind speed, a southward IMF turning may have a strong influence on relativistic electron enhancement (Blake et al. 1997; Miyoshi et al. 2013). The southward IMF evidently stimulates the substorm activity and energetic electron injection into the magnetosphere. The occurrence of substorm during the storm recovery phase was proposed as a necessary condition for the ORB flux increase (Antonova et al. 2018).

In collisionless near-Earth plasma charged particles can gain or lose energy only due to the interaction with electromagnetic waves. Thus, possible mechanisms of electron acceleration in the Earth's magnetosphere are caused by resonant wave–particle interaction with ultra-low-frequency (ULF) and very low-frequency (VLF) waves. The resonant interaction of ULF waves in the Pc5 frequency band with energetic electrons results in the earthward radial diffusion and the electron acceleration due to the betatron mechanism. The resonant interaction can take place with azimuthally large-scale ($1 < m < 10$) Alfven waves (toroidal mode) via drift resonance, when the wave period matches the multiple of the electron drift period, $\omega = m\omega_d$ (ω is the wave frequency, m is the azimuthal wave number, and ω_d is the electron drift frequency) (Elkington et al. 1999; Liu et al. 1999; O'Brien et al. 2001; Shprits et al. 2008a). Toroidal Pc5 pulsations are mostly generated by the Kelvin–Helmholtz shear flow instability on the magnetopause or excitation of the

cavity/waveguide mode by the solar wind buffeting of the magnetopause, with subsequent field-line resonant (FLR) amplification inside the magnetosphere (Kivelson and Pu 1984; Nopper et al. 1982; Pilipenko et al 2010). Besides, azimuthally small-scale waves (poloidal mode, $m >> 10$) can also lead to the electron acceleration via the drift-bounce resonance $\omega - m\omega_d = k\omega_b$ (ω_b is the particle bounce frequency; k is an integer, usually ± 1) (Ukhorskiy et al. 2009). The mechanism of the acceleration of seed energetic electrons supplied by substorms may be visualized as the magnetospheric geosynchrotron, where ULF disturbances resonantly pump energy into orbiting electrons in the magnetospheric trap.

Interplanetary shock arrival preceding the magnetic storm causes rapid compression of the magnetosphere and produces a variety of phenomena (Belakhovsky et al. 2017). Among them is the rapid electron enhancement produced by the inward radial diffusion leading to the violation of the third adiabatic invariant (Kanekal et al. 2016; Hudson et al. 2017; Hao et al. 2019).

The acceleration of electrons injected into the magnetosphere may be closely associated with the substorm development. Indeed, the amount of energy contained in the ORB electrons is smaller than the amount of energy released in a typical substorm by orders of magnitude, thus only a small fraction of the substorm energy is required to power the seed electrons. Rapid increases in ~ hour time interval of electron fluxes during substorm activation are caused by radial injection owing to impulsive electric fields induced during magnetic field dipolarization (Lazutin 2013). However, the injection process is not sufficient to completely populate the ORB (Baker and Daglis 2007). Nonetheless, an impulsive injection of seed energetic (up to ~ 100 keV) electrons into the ORB heart during substorms is possibly the necessary condition for the ORB enhancement.

The VLF chorus emissions are another plausible agent of the energetic electron acceleration (Summers et al. 1998; Shprits et al. 2008b; Thorne et al 2013). Chorus waves are intense whistler mode electromagnetic emissions characterized by a sequence of discrete elements in the range of 0.1–0.8 f_e (f_e is equatorial electron cyclotron frequency), often with a gap around 0.5 f_e (Tsurutani and Smith 1977). Chorus emissions have some very particular property that makes them effective: they occur outside the plasmapause in a fairly narrow frequency band and propagate away from the magnetic equator where they are generated. Their source is the instability of electrons with energy ~ tens of keV injected during substorms, so the chorus emission intensity closely correlates with the substorm activity (Meredith et al. 2002; Jaynes et al. 2015; Takahashi et al. 2021). The excited chorus emission supposedly accelerates locally electrons with ~ hundreds of

Belakhovsky *et al. Earth, Planets and Space* (2023) 75:189

Page 4 of 17

keV to MeV energies. Indeed, strong correlation between VLF chorus and relativistic electron fluxes was observed by Van Allen probes (Thorne et al. 2013). The influence of VLF chorus was found to be strongly L-dependent, being most efficient at L-shells inside the geostationary orbit. Thus, VLF chorus emission operates as an intermediary transferring energy from low-energy electrons to higher-energy electrons. Possibly, the ULF and VLF acceleration mechanisms may produce synergetic impact on the ORB dynamics providing a significantly larger effect than their separate actions.

Strong depression of magnetospheric magnetic field during the storm onset provides an adiabatic decrease of the electron fluxes, but they should recover to the pre-storm level upon restoration of the magnetic field. However, Tverskoy (1997), and later Antonova (2006), indicated a possibility of the ORB belt energization during this process. Seed electrons cast into a region with a weak magnetic field depressed by the ring current, upon the magnetospheric magnetic field recovery must undergo subsequent betatron acceleration. This mechanism was claimed to interpret the relationship between the position of the radiation belt maximum after storm L_{max} and maximum of Dst variation during storm (Tverskaya 1996; Tverskaya et al. 2005) as follows (Antonova and Stepanova 2015; Antonova et al. 2018; Moya et al. 2017; Boyd et al. 2018; Stepanova et al. 2021)

$$|\text{Dst}|_{max} = 2.75 \cdot 10^4 L_{max}^{-4} \text{ or } |\text{SYM - H}|_{max} = 3.0 \cdot 10^4 L_{max}^{-4} \tag{1}$$

According to this conception, the stronger magnetic storm is, the deeper ORB maximum is located after it.

Most probably several mechanisms are involved in the ORB electron energization at different phases of magnetic storm, but the actual contribution of each of them is not known yet. In this paper, we try to estimate the contribution of the three above mechanisms (ULF, VLF, and adiabatic) into the acceleration of ORB electrons up to the relativistic energies for several events using Arase and GOES satellite data.

Data used and methods

The electron fluxes data in wide energy range (from tens of keV to some MeV) were provided by Arase (ERG) satellite and geostationary GOES mission. The Energization and Radiation in Geospace (ERG) project is designed to explore the Earth's radiation belt, where relativistic-energy electrons with energies of the order of MeV are generated from considerably lower-energy populations, such as solar wind electrons with energy of hundreds of eV and electrons from ionospheric sources with sub-eV energy (Miyoshi et al. 2018). The Arase/ERG satellite was developed by the Japan Aerospace Exploration Agency (JAXA) in collaboration with universities and institutes in Japan and Taiwan. The essential key observation of this program entails to conduct in situ measurements of particles and electromagnetic fields in the ORB (Miyoshi et al. 2018). Arase initiated its scientific observation on March 24, 2017. Given its perigee altitude of ~400 km and its apogee altitude of ~32,000 km, Arase can cover the entire ORB in its orbit. The orbit inclination is ~31° and orbital period is ~570 min. We have analyzed data from XEP-e (extremely high-energy electron sensor, 0.4–20 MeV) instrument (Higashio et al 2018), and MEP-e (Medium-energy particle sensor – electron, 7–87 keV) instrument (Kasahara et al. 2018a, b). Additionally, we have used the data on fluxes of electrons with different energies (40, 75, 475 keV, > 0.8, and > 2 MeV) from geosynchronous satellites GOES-13, -15.

The solar wind and interplanetary magnetic field (IMF) parameters are taken from the OMNI database. The geomagnetic indices at hand, SYM-H and AE, characterize magnetic storm intensity and substorm activity. We have also calculated the corrected SYM-H* index values (Kozyra et al. 2002) to reduce a contribution from the magnetopause currents.

To quantify the global wave activity in the Pc5 band (2–7 mHz) we use the planetary ULF wave power index (Pilipenko et al. 2017). This index is calculated from the world-wide magnetometer array data, and it is a proxy of large-scale magnetospheric disturbances in the Pc5 band. The ionosphere is a natural filter that screens the ground magnetometers from small-scale magnetospheric disturbances (e.g., poloidal Pc5 waves with large azimuthal wave numbers $m > 20$).

As a proxy of the VLF activity in the magnetosphere we have used data from PWE (plasma wave experiment) instrument on Arase satellite. The PWE sensor records electric fields in the frequency range from DC to 10 MHz and magnetic fields in the frequency range from a few Hz to 100 kHz (Kasahara et al. 2018a, b). The electric field component is measured by two pairs of wire dipole antennas with a tip-to-tip length of 30 m, and the magnetic field component is measured using three-axis search coils. The OFA subcomponent (Matsuda et al. 2018) of the PWE produces the power spectrum as well as the spectrum matrix for both electric and magnetic fields from 10 Hz to 20 kHz. The time resolutions of the power spectrum and spectrum matrix are

Belakhovsky *et al. Earth, Planets and Space* (2023) 75:189

Page 5 of 17

nominally 1 and 8 s, respectively, while the possible time resolutions are 0.5–4 s and 4–32 s, respectively. We have summarized VLF wave intensity in frequency range 0.7–4.54 kHz which is typical for the chorus wave activity.

The advantage of Arase orbit is the possibility to cross the region of the ORB maximum with time resolution ~ 2.4 h which provides a comparatively good possibility for the analysis of its temporal dynamics. Using data from Arase and GOES satellites, solar wind monitors, and ground-based observations we analyze the electron acceleration processes during selected space weather activation periods and try to reveal contributions of various mechanisms in the ORB response.

The comparative analysis of the storm and non-storm periods

We analyze 3 geomagnetic storms that are among strongest during the Arase satellite epoch: May 27–29, 2017 (Dst = − 125 nT), September 7–10, 2017 (Dst = − 122 nT), and August 25–28, 2018 (Dst = − 175 nT). These storms are caused by the coronal mass ejection (CME) and are preceded by the storm sudden commencement (SSC). We have also considered the non-storm periods (|Dst| < 50 nT) with a high solar wind speed before and after these storms. Figure 1 shows the location of the Arase satellite in the equatorial XY plane (GSM coordinate system) during those three events.

We compare storm interval with non-storm interval (with high solar wind speed) to find whether the level of relativistic electrons depends on geomagnetic storm intensity or not. The Tveskoi mechanism of electron acceleration is related to the intensity of the geomagnetic storm. We also try to find out whether the speed of the solar wind alone (even without magnetic storm) affects the fluxes of relativistic electrons. Since the solar wind

speed is the main factor for the generation toroidal Pc5 pulsations in the magnetosphere.

May–June 2017

We have selected two time intervals: the non-storm period with a high solar wind speed (May 15–26) and the geomagnetic storm (27 May–2 June). The storm and non-storm intervals are highlighted in red and green on variations of SYM-H index, respectively (Fig. 2). During the non-storm time interval, the solar wind speed V experiences two enhancements: during the first one V reaches ~ 600 km/s, during the second one V reaches ~ 760 km/s (Fig. 2, panel 9). All the time SYM-H index keeps at the level about − 30 nT (Fig. 2, panel 5). The arrivals of the fast solar wind streams are preceded by jumps of the solar wind density up to $N \sim 60$ cm^{-3}. During non-storm interval the IMF Bz-component varies from negative to positive values, − 10/+5 nT (Fig. 3, panel 6).

During the storm, SYM-H index drops to -142 nT (Fig. 2, panel 5), and the solar wind speed, ~ 400 km/s, becomes lower than that during the non-storm interval, and only after the storm V reaches ~ 500 km/s (Fig. 2, panel 9). The storm onset is preceded by the strong jump of the solar wind density up to 60 cm^{-3} (Fig. 2, panel 10). The IMF Bz-component keeps southward, about −20 nT, during about 20 h (Fig. 3, panel 6) which enables the solar wind energy to penetrate inside the Earth's magnetosphere. It was CME (coronal mass ejection) geomagnetic storm since this storm were accompanied the storm sudden commencement.

Figure 2 (panels 1–3) shows variations of the electron fluxes with different energies: 40 keV ("seed" electrons), 475 keV (sub-relativistic electrons), and > 2 MeV (relativistic electrons). Daily variations in fluxes of relativistic electrons are not seen in fluxes of 40 and 475 keV
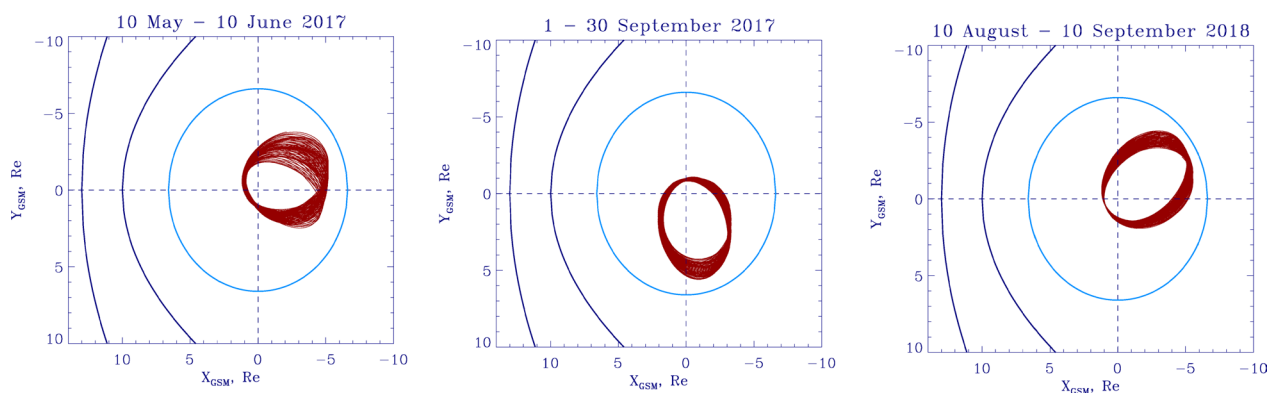

Fig. 1 The orbits of the Arase satellite in XY plane of the GSM coordinate system: 10 May–10 June 2017 (left-hand panel), 1–30 September 2017 (central panel), and 10 August–10 September 2018 (right-hand panel)
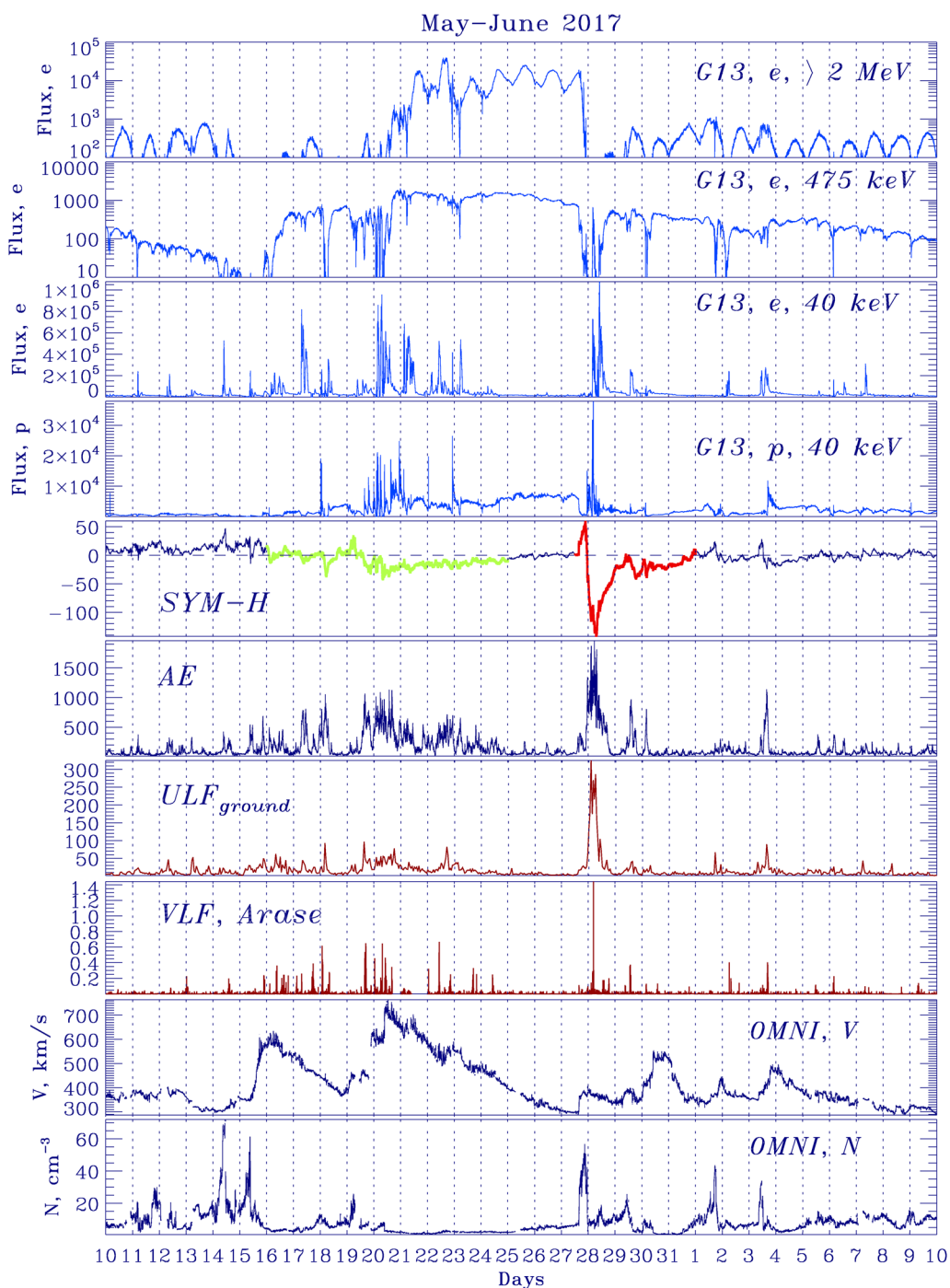
Fig. 2 The electron fluxes on GOES-13, solar wind parameters, indexes of geomagnetic activity on 10 May 2017–10 June 2017. The variations of GOES-13 electron fluxes with energy $E > 2$ MeV (first panel), with energy $E = 475$ keV (second panel), with energy $E = 40$ keV (third panel); SYM-H index, AE-index; OMNI solar wind velocity V, OMNI solar wind density N; ULF power index, VLF power intensity (0.7–4.54 kHz) according to Arase satellite on 10 May–10 June 2017. The green line on variations of SYM-H index is non-storm interval, red line is storm interval

electrons. The fluxes of the relativistic electrons start to grow tens of hours after the growth of 40 keV and 475 keV electron fluxes. The flux of the relativistic electrons abruptly decreases between 27 and 28 May after the jump of the solar wind density (before the onset of magnetic storm). Possibly, it caused by geosynchronous magnetopause crossing or by adiabatic Dst-effect (Li et al. 1997).
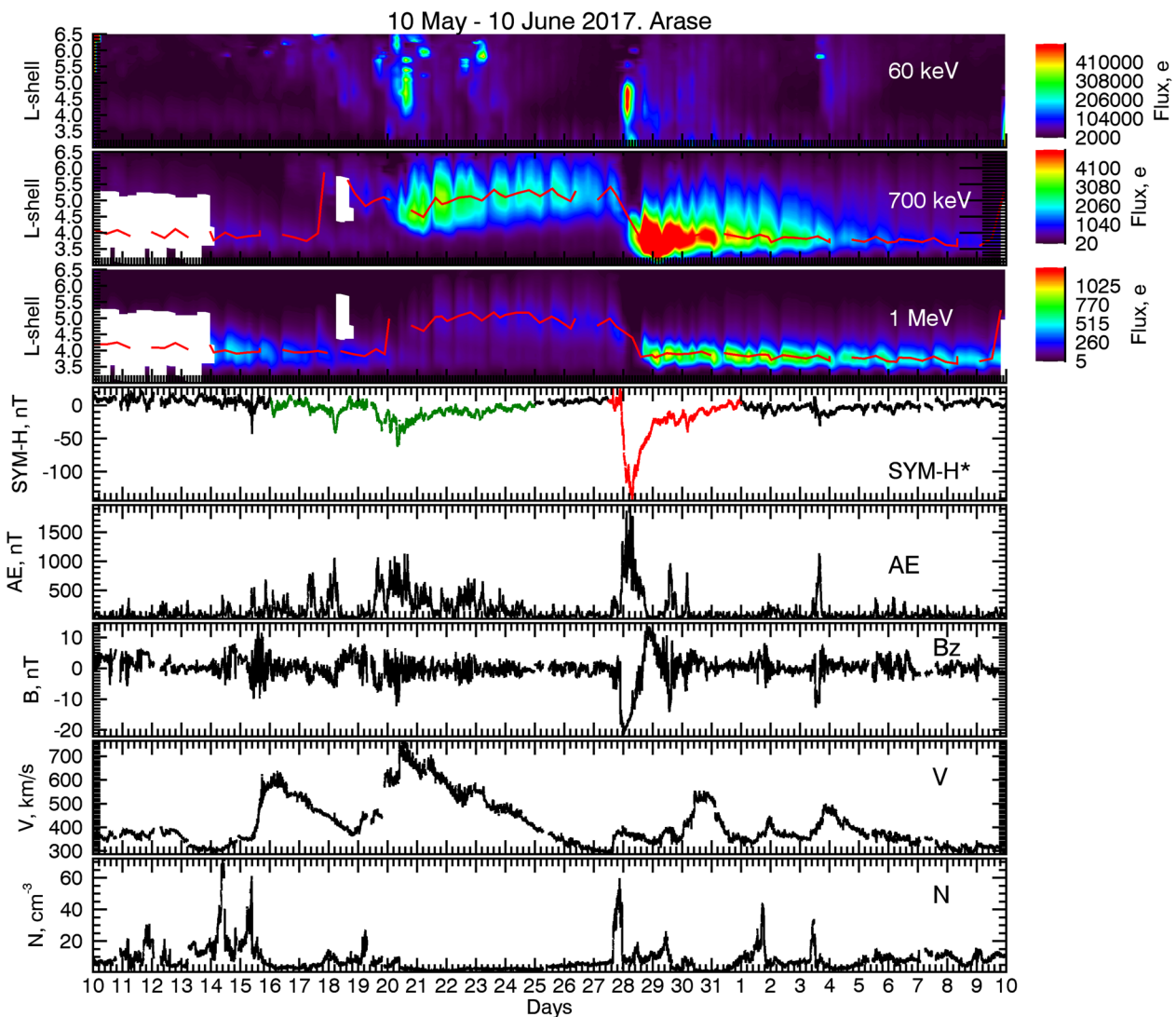
Belakhovsky *et al. Earth, Planets and Space* (2023) 75:189

Page 7 of 17

Fig. 3 The electron fluxes on Arase, indexes of geomagnetic activity, solar wind parameters on 10 May 2017–10 June 2017. Variations of electron fluxes on Arase with energy *E* = 60 keV (first panel), with energy *E* = 700 keV (second panel), with energy *E* = 1 MeV (third panel); SYM-H* index, AE-index; Bz-component of the IMF, solar wind velocity V, solar wind density N according to the OMNI database on 10 May–10 June 2017. The green line on variations of SYM-H* index is non-storm interval, red line is storm interval

At the geostationary GOES-13 orbit the peak level of relativistic electron fluxes during non-storm interval ($>10^4$ 1/(eV cm^2 s str)) on 20–25 May is greater than that during the strong geomagnetic storm ($<10^4$ 1/(eV cm^2 str)). Thus, at the geosynchronous Earth orbit (GEO) the geomagnetic storm intensity is not a decisive factor of the relativistic electron level, whereas the solar wind speed determines primarily the relativistic electron energization. This congestion is consistent with the ULF generation mechanisms, because the magnetospheric ULF wave power is well known to grow directly in response to the solar wind speed.

The high level of relativistic electrons coincides in time with the high level of energetic 40 keV protons (Fig. 2, panel 4) till May 27. The proton injection may stimulate the excitation by kinetic instabilities of storm-time Pc5 pulsations, though GOES-13 has not detected them.

The rapid growth of the 40 keV ("seed") electrons occurs simultaneously with the increase of AE index (Fig. 2, panel 6). The relevant substorm activation coincides in general with the growth of ULF and VLF activities in the magnetosphere, as evident from the ULF index (Fig. 2, panel 7) and VLF power (Fig. 2, panel 8) behavior. The growth of the magnetospheric ULF activity is possibly stimulated by the jump of the solar wind density,

Belakhovsky *et al. Earth, Planets and Space* (2023) 75:189

Page 8 of 17

though the solar wind speed during this moment is not very high (< 400 km/s).

The Arase data give a possibility to examine how the electron fluxes (60 keV, 700 keV, and 1 MeV) vary at different L-shells (Fig. 3). The Arase orbit from May 10 to June 10 lies in the midnight and morning sectors (Fig. 1, left panel). The red line shows the location of the ORB maximum (Fig. 3). The 60 keV electrons start to grow at higher L-shells than the MeV electrons do. The total level of the 1-MeV relativistic electron fluxes during geomagnetic storm is much greater than during non-storm period in contrary to the GEO observations. The maximum of the relativistic electron fluxes shifts during geomagnetic storm to lower L-shells ($L \approx 3.5$–4) as compared with the non-storm period ($L \approx 5$). We calculated the SYM-H* index which does not include the contribution of the magnetopause current to the SYM-H index. The red color on variations of the SYM-H index is storm interval, green color is non-storm interval. However, the value of SYM-H* during non-storm interval is less than − 50 nT. So, possibly, this is CIR magnetic storm.

The above analysis has shown that on the initial phase the simultaneous increase of the ULF and VLF activities contribute to the electron acceleration. After that, the relativistic electron fluxes keep nearly on the same level during about ten days. After initial phase of electron acceleration, the recovering magnetospheric magnetic field can also contribute to electron energization due to the betatron mechanism. The efficiency of the betatron mechanism is characterized by variations of SYM-H* index. During the storm time interval, the depression of the magnetospheric magnetic field is much greater than that during the non-storm interval (Fig. 3, panel 4). In line with that, the level of relativistic electron flux during the magnetic storm is substantially greater than that during the non-storm interval (Fig. 3). Additionally, we have estimated the relationship like (1) and found that $|SYM\text{-}H|_{max}^* L_{max}^4 \sim 2.8 \cdot 10^4$. The obtained relationship is rather close to (1), the difference may indicate that other mechanisms are involved in the electron acceleration except Tverskoi mechanism.

For this geomagnetic storm during the initial phase of electron acceleration the solar wind speed is not high (~ 400 km/s), the relativistic electron fluxes reach a high level at lower L-shells. The solar wind density increase can also generate ULF waves in magnetosphere (Takahashi et al. 2021) due to FLR or cavity/waveguide mode. Therefore, we suggest that a high solar wind velocity is not always a necessary factor for the relativistic electron growth. At the same time, the substorm activity intensity is the important factor for the ORB enhancement.

September 2017

During this strong magnetic storm (SYM-H $\approx$ -150 nT), AE index reaches extreme values ~ 2700 nT (Fig. 4, panels 5 and 6), the solar wind speed has extreme values ~ 860 km/s (Fig. 4, panel 9), and the IMF Bz-component is less than -30 nT (Fig. 5, panel 6). There are two main phases of the storm since the IMF Bz-component has an excursion to positive values. During the second main phase the SYM-H index reaches about − 120 nT.

Unlike the previous event, the non-storm interval with a high solar wind speed is observed after the storm on September, 14–21. The storm and non-storm intervals are highlighted in red and green on variations of SYM-H index, respectively (Fig. 4, panel 5). During the non-storm period the solar wind speed (V < 700 km/s) is less than that during the storm period, but has such values during a long time, > 3 days (Fig. 4, panel 9). AE index is also elevated (> 1000 nT) during a long time, from September, 14 to September, 18. A high level of AE index during a long time suggests that such period can be the High Intensity Long Duration Continuous AE Activity (HILDCAA) event.

Figure 4 (panels 1–3) shows variations of the electron fluxes with energies 40 keV, 700 keV, > 2 MeV at GOES-13 satellite. Daily variations are not pronounced in fluxes of 40 and 475 keV electrons. At the geostationary orbit the magnetic storm causes dropout of relativistic electrons with a subsequent recovery to the pre-storm level. The relativistic electron fluxes start to increase some days after the growth of 40 keV and 475 keV electrons. The growth of energetic (40 keV and 475 keV) electrons, and relativistic (> 2 MeV) electrons occurs during tens of hours. The high level of relativistic electrons coincides in time with the high level of energetic 40 keV protons (Fig. 4, panel 4) till September 22. During both non-storm and storm time intervals, the growth of ULF index coincides with the growth of AE index and VLF activity (Fig. 4, panels 6–8). Therefore, it is not easy to separate the contribution of ULF and VLF acceleration mechanisms over time.

At the geosynchronous orbit, the level of the relativistic electron fluxes during the non-storm interval (> 10^4 1/(eV cm^2 s str)) is much greater than that during the strong magnetic storm (< 10^4 1/(eV cm^2 s str)). Variations of the electron fluxes (60 keV, 700 keV, and 1 MeV) at different L-shells as observed by Arase are shown in Fig. 5. The Arase orbit from 1 to 30 September lies in the evening sector (Fig. 1, center panel). The red line on the second and third panels marks the locations of the electron flux maxima. The maximum of relativistic electrons (1 MeV) shifts to lower L-shell ($L \approx 3.5$) than during events in May 2017 (Fig. 5, panel 3). During the non-storm interval, the maximum of relativistic electrons is located at $L \approx 4.5$
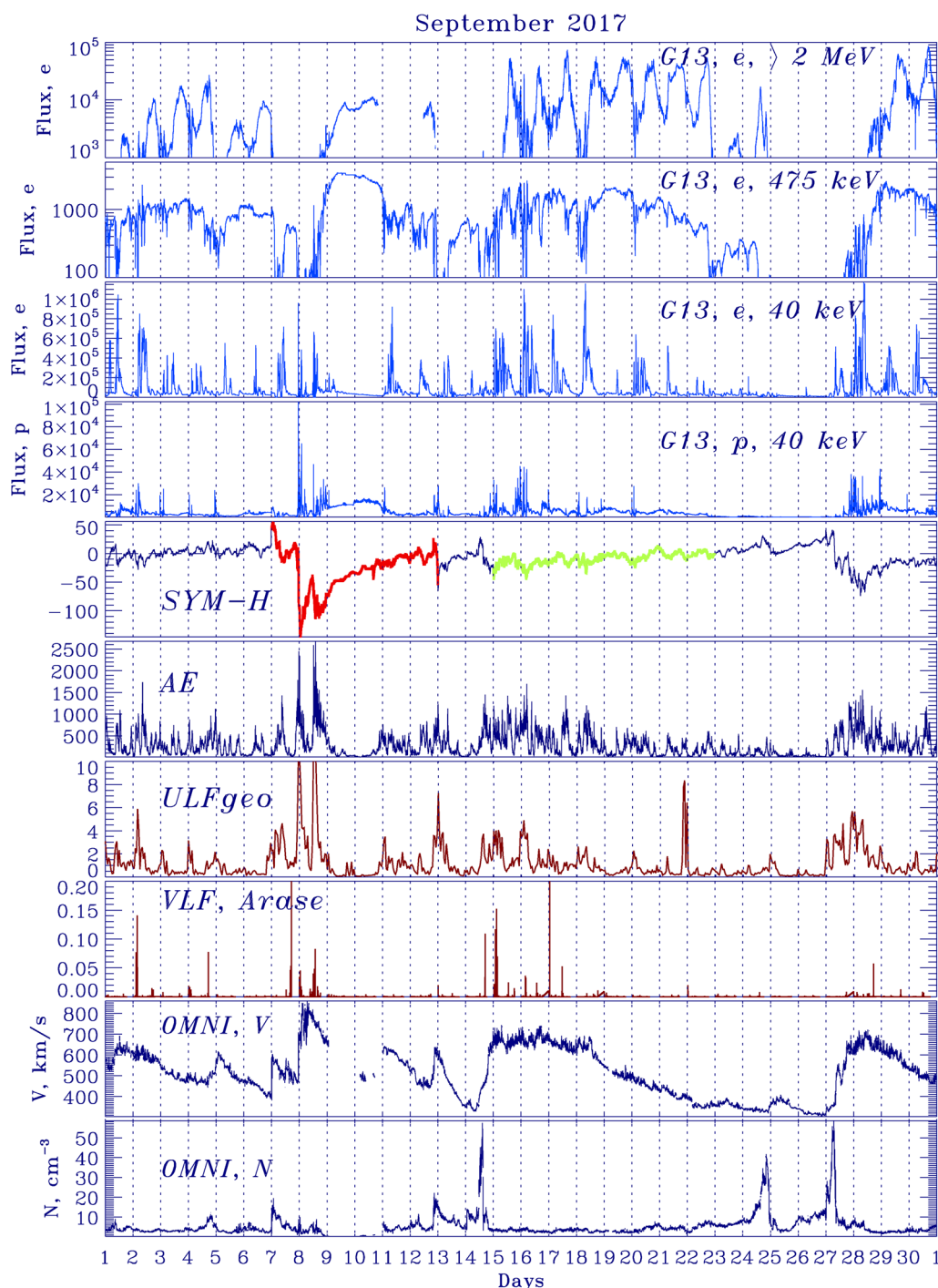
Fig. 4 The electron fluxes on GOES-13, solar wind parameters, indexes of geomagnetic activity on 1–30 September 2017. The variations of GOES-13 electron fluxes with energy $E > 2$ MeV (first panel), with energy $E = 475$ keV (second panel), with energy $E = 40$ keV (third panel); SYM-H index, AE-index; OMNI solar wind velocity V, OMNI solar wind density N; ULF power index, VLF power intensity (0.7–4.54 kHz) according to Arase satellite on 1–30 September 2017. The green line on variations of SYM-H index is non-storm interval, red line is storm interval

(Fig. 5, panel 3). The total level of the relativistic electron flux during the storm is much higher than that during the non-storm interval.

During this event the increase of ULF and VLF activities occurs practically simultaneously, so on the initial phase both mechanisms may provide contribution to electron acceleration. At later phase, the recovering
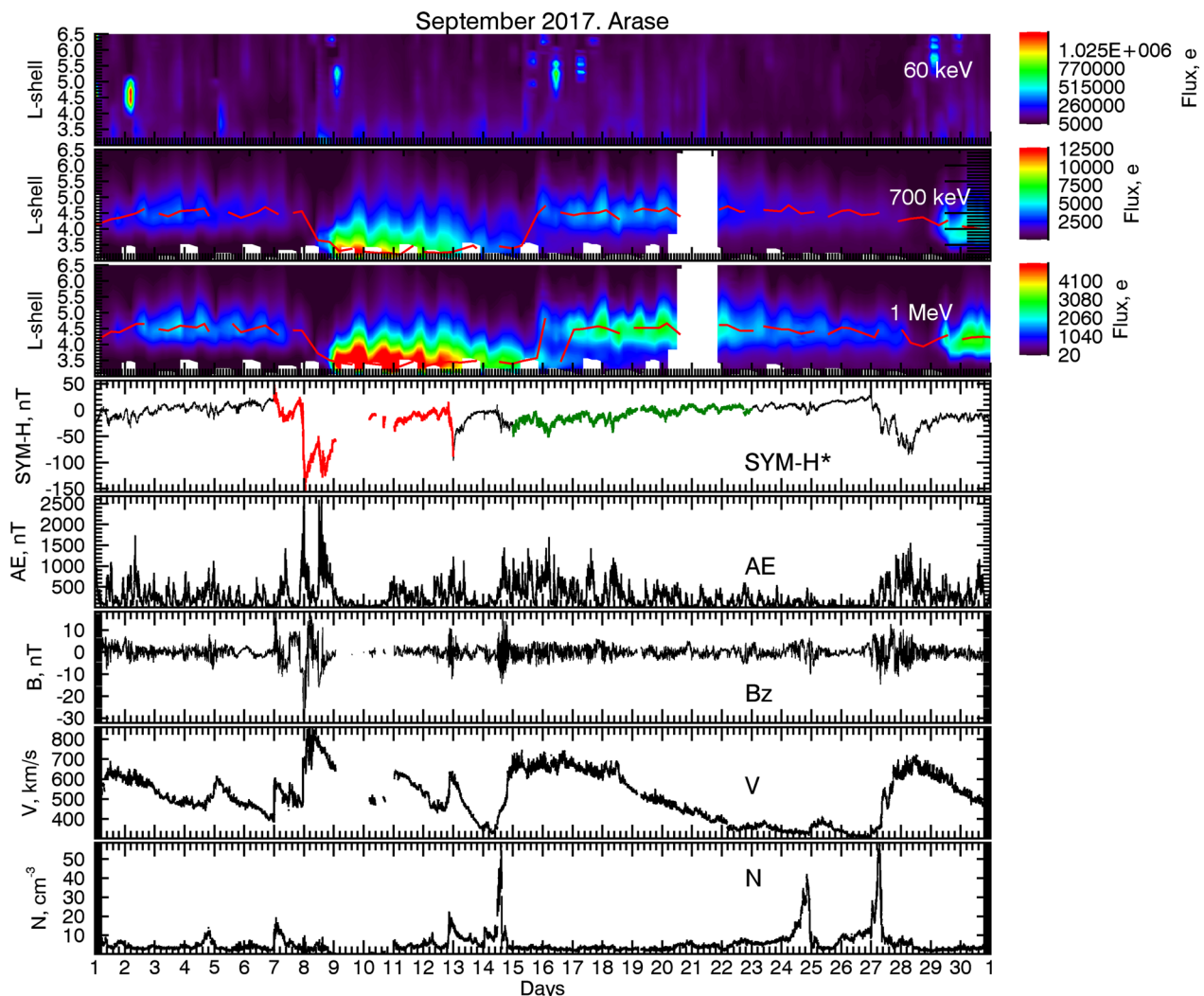
Fig. 5 The electron fluxes on Arase, indexes of geomagnetic activity, solar wind parameters on 1–30 September 2017. Variations of electron fluxes on Arase with energy $E = 60$ keV (first panel), with energy $E = 700$ keV (second panel), with energy $E = 1$ MeV (third panel); SYM-H* index, AE-index; Bz-component of the IMF, solar wind velocity V, solar wind density N according to the OMNI database on 1–30 September 2017. The green line on variations of SYM-H* index is non-storm interval, red line is storm interval

magnetic field can provide an additional electron acceleration due to the betatron mechanism. However, the obtained relationship $|SYM\text{-}H|_{max} * L_{max}^{4} \sim 2.10^{4}$ for this event deviates significantly from the relationship (1). This discrepancy may indicate that besides the betatron mechanism other mechanisms are still involved in the electron acceleration. The increase of relativistic electrons at larger L during HILDCAA period can be provided by ULF waves, stimulated by increased solar wind velocity and substorm activity.

August–September 2018
During this storm on August 26–September 2, SYM-H index drops to -210 nT. During pre-storm interval

16–23 August SYM-H index is about -40 nT, while the solar wind speed ($V \sim 670$ km/s) is somewhat higher than during the storm ($V \sim 630$ km/s) (Fig. 6, panel 5). However, the substorm activity is much stronger during the storm (AE ~ 2200 nT) than during the non-storm interval (AE ~ 1200–1300 nT). During the storm the IMF Bz-component is southward for ~ 18 h at the level about -16 nT (Fig. 7, panel 6). During the initial storm phase, the solar wind density jumps up to $N \sim 34$ cm^{-3}.

Unlike the previous two events, at the geostationary orbit after the storm the level of relativistic electron flux, $> 10^{5}$ 1/(eV cm^{2} s str), is higher than after the non-storm interval, $< 10^{5}$ 1/(eV cm^{2} s str) (Fig. 6, panel 1). Gradual growth of the energetic (40 keV and 475 keV)
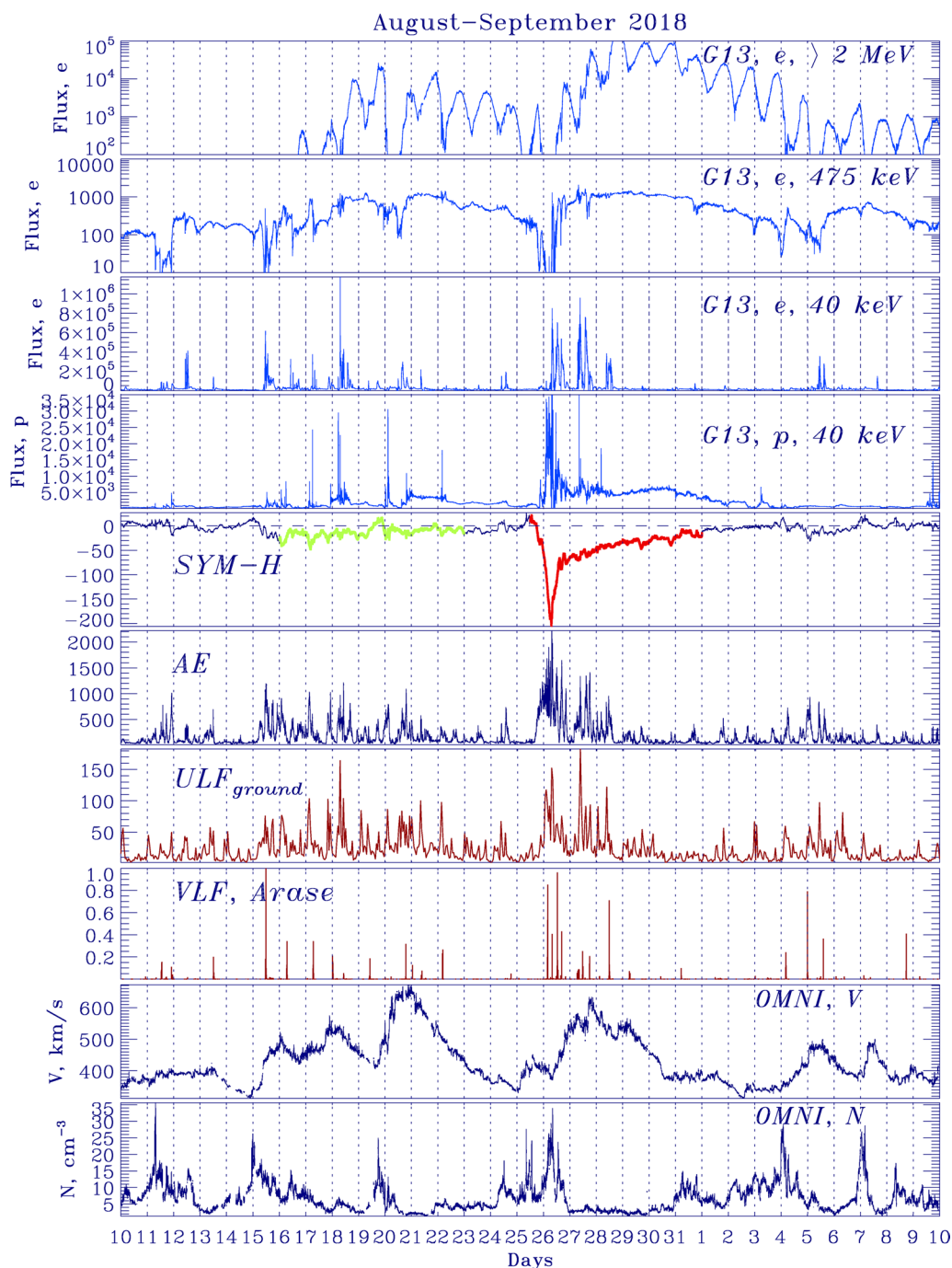
Fig. 6 The electron fluxes on GOES-13, solar wind parameters, indexes of geomagnetic activity on 10 August–10 September 2018. The variations of GOES-13 electron fluxes with energy $E > 2$ MeV (first panel), with energy $E = 475$ keV (second panel), with energy $E = 40$ keV (third panel); SYM-H index, AE-index; OMNI solar wind velocity V, OMNI solar wind density N; ULF power index, VLF power intensity (0.7–4.54 kHz) according to Arase satellite on 10 August–10 September 2018. The green line on variations of SYM-H index is non-storm interval, red line is storm interval

electrons and relativistic electrons (>2 MeV) occurs for tens of hours (Fig. 6, panels 1–3). The growth of the ULF index and VLF activity coincides with the growth of the

AE index during both non-storm and storm time intervals (Fig. 6, panels 6–8).

The Arase orbit from August 10 to September 10 lies in the postmidnight-evening sector (Fig. 1, right panel).
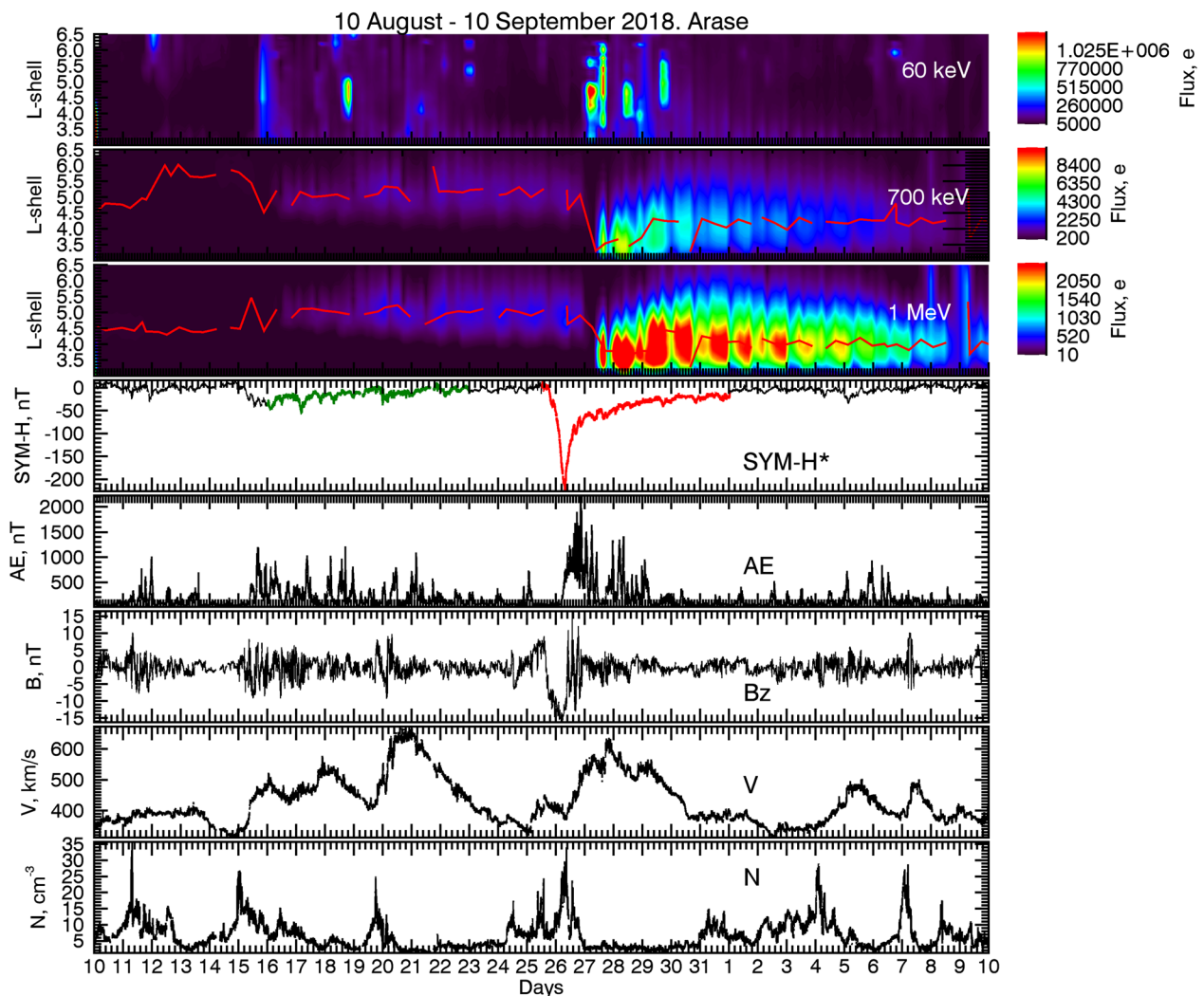
Fig. 7 The electron fluxes on Arase, indexes of geomagnetic activity, solar wind parameters on 10 August–10 September 2018. Variations of electron fluxes on Arase with energy $E = 60$ keV (first panel), with energy $E = 700$ keV (second panel), with energy $E = 1$ MeV (third panel); SYM-H* index, AE-index; Bz-component of the IMF, solar wind velocity V, solar wind density N according to the OMNI database on 10 August–10 September 2018. The green line on variations of SYM-H* index is non-storm interval, red line is storm interval

The satellite records the 60 keV electron flux growth at wider and higher L-shells than the growth of MeV electrons. The maximum of the relativistic electrons (1 MeV) is found to be located at $L \approx 3.5$–4, whereas during non-storm interval the ORB maximum is located at $L \approx 5$ (Fig. 7, panel 3). The total level of the relativistic electron flux during the storm is higher than that during the non-storm interval both at the geostationary orbit and at lower L-shells (Fig. 7, panel 3). For this event the solar wind speed has comparable values during both storm and non-storm intervals, but AE index during storm interval is nearly 2 times higher than during non-storm interval. A higher electron energization rate during the storm period is probably due to a higher level of substorm activity. The increase of the ULF and VLF activities in the magnetosphere practically coincide, therefore ULF waves and VLF emissions may both provide a contribution to the electron acceleration on the initial phase.

The additional betatron acceleration mechanism may operate upon the magnetospheric magnetic field recovery at the later phase. However, the estimated relationship $|\text{SYM-H}|_{max} * L_{max}^4 \sim 4.56 * 10^4$ deviates considerably from the relationship (1). Thus, the scenario of seed electron injection into the region of depressed magnetic field probably operates simultaneously with ULF and VLF associated mechanisms. A reliable verification of this scenario requires more careful analysis of the ring current distribution and dynamics.

Discussion

In this paper, we have examined 3 strong magnetic storms with different intensities and the non-storm intervals with a high solar wind speed before and after storms to reveal a possible contribution of different mechanisms into the electron acceleration in the Earth magnetosphere. These storms are caused by CMEs since their intensity is high, $Dst < -100$ nT, and they are preceded by SSC (Borovsky and Denton 2006). We focus on case study which can shed light on some aspects that cannot be revealed in statistical study. Besides popular ULF and VLF mechanisms of electron energization, we have considered also the betatron mechanism associated with the magnetic field recovery.

We have examined the contribution of ULF and VLF activities into the relativistic electron acceleration using as the activity measures the ULF wave power index derived from ground-based magnetometer data and the VLF power from Arase satellite. Other teams used different measures for describing ULF/VLF activities and space weather conditions. O'Brien et al. (2003) to characterize the chorus wave activity used MeV electron microbursts detected by the low-altitude SAMPEX satellite. They concluded that in the inner magnetosphere ($L \sim 4.5$) the relativistic electron energization is likely caused by VLF/ELF wave acceleration, while ULF activity probably produces the dominant acceleration at the geosynchronous orbit and beyond. Katsavrias et al. (2015) following Li et al. (2013) for describing VLF emission activity used electron flux data over the energy of 30–100 keV from the low-altitude POES satellites. To characterize the ULF activity, they used magnetic field measurements at RBSP satellites. They found that the contributions of ULF and VLF activities into the relativistic electron acceleration were different for different events. Simms et al. (2016) used ground ~1 kHz VLF measurements at Halley station (Antarctica) at the dawn sector to characterize the VLF activity in the magnetosphere. However, this approach is not very reliable, because some VLF chorus emissions are confined near the equator and do not propagate to the ground. Simms et al. (2018) used DEMETER satellite measurements for describing the VLF activity and the ground ULF index. They constructed the regression model which showed that ULF waves and VLF chorus emissions exerted approximately the same impact on relativistic electron flux at two lower energy channels (0.7–3.5 MeV), whereas at higher energies the chorus influence remained strong while the ULF Pc5 influence drops off. Simms et al. (2021) using regression analysis showed that over $L = 4$–6 both chorus and ULF Pc5 correlated with immediate electron decreases and delayed enhancement, whereas ULF waves consistently showed a stronger influence on electron enhancement than chorus waves did. Capman et al. (2019) using multiple and logistic regression analysis determined among different factors, such as ULF waves, VLF emissions, EMIC waves, seed electron, Dst index, substorm occurrence, and solar wind input, the most essential factors for the relativistic electron dynamics at the geostationary orbit. They claimed that the most influential were ULF Pc5 waves and the seed electrons.

Statistical studies (Lyatsky and Khazanov 2008; Simms et al. 2016; Kim et al. 2015; Pinto et al. 2018) proved a poor correlation between Dst index and growth of MeV electrons at geostationary orbit. Our analysis of the Arase data proved that the maximum of MeV electron distribution over L-shells shifts deeper into the magnetosphere during geomagnetic storms. So during recovery phase of the magnetic storms adiabatic mechanism can have contribution to the electron acceleration (Antonova and Stepanova 2015).

Our observations have shown the presence of the intense 40 keV proton fluxes on GOES satellite during the relativistic electron growth. This correspondence may be considered as indirect indication on a possible contribution of storm-time Pc5 pulsations generated by the ring current proton instability to the electron acceleration (Ukhorskiy et al. 2009).

The examination of the May 27–30, 2017 storm has shown that a high solar wind velocity is not an obligatory condition for the relativistic electrons growth. In line with that, Reeves et al. (2011) based on 20 years LANL satellite data showed that correlation between the solar wind velocity and flux of MeV electrons was complex and not linear.

A powerful tool for the study of the electron evolution upon changes of the magnetospheric magnetic field is the phase space density (PSD) calculated in the space of adiabatic invariants. In accordance with (Reeves et al. 2013), radial diffusion driven by ULF waves produces a smoothing of the PSD radial profile, while the VLF mechanism produces a local PSD peak where the resonant interaction occurs. The PSD radial profiles from Van Allen probes showed that local acceleration was the dominant acceleration mechanism for MeV electrons in the ORB, whereas 87% of the enhancement events exhibited localized peaks (Boyd et al. 2018). The calculation of PSD requires an accurate magnetic field model (Reeves et al. 2013), while substorm injections can produce temporal changes of the magnetic field geometry which cannot be adequately described by existing models. Therefore, the absence of definite information about the global changes of the magnetic field creates an uncertainty in the analysis results.

During the storm main phase, the ORB is partly depleted, and energization of relativistic electrons by

Belakhovsky *et al. Earth, Planets and Space*   (2023) 75:189

Page 14 of 17

several orders of magnitude takes place during a recovery phase on the background of a high solar wind stream and extended substorm activity. These conditions favor the excitation of both ULF waves and VLF emissions. The electron fluxes reach largest magnitudes about 1–2 days after the appearance of high solar wind streams. Miyoshi and Kataoka (2005) found that on average CIR-associated storms were more effective in the MeV electron flux enhancement at the geosynchronous orbit than CME storms. Energetic electrons (50–100 keV) injected during substorms serve as seed particles for a subsequent acceleration of a group of these electrons up to relativistic energies. The injection of energetic electrons also stimulates the excitation of VLF emissions. Thus, a substorm activity is one of the necessary conditions for the appearance of killer-electrons in the magnetosphere.

A radial diffusion of seed electrons inside the geosynchronous orbit is stimulated by elevated level of ULF waves and fluctuations. Upon the diffusion into the regions with a more intense magnetic field electrons are betatron-accelerated. Thus, ULF activity operates as a "supplier" of pre-accelerated energetic electrons into the ORB. In the inner magnetosphere these electrons are locally accelerated due to resonant interaction with VLF chorus emissions. It was found (Foster et al. 2017) that chorus waves can accelerate seed electrons by 50–200 keV in resonant nonlinear interactions on a time scale of 10–100 ms.

Indeed, a statistical multi-factor analysis showed that synergetic influence of ULF and VLF powers on electron fluxes is higher than a sum of separate influence of those two factors (Simms et al. 2016). Whistler-mode chorus waves are often modulated by ULF waves. It was found periodic excitations of lower- and upper-band chorus waves near ULF wave crests and troughs, respectively (Li et al. 2023).

However, the electron energization can take place without ULF or VLF wave activity involved. According to Tverskoy (1997) scenario, during the storm main phase an injection of energetic electrons into a region with a depressed magnetic field occurs, then upon a recovery of magnetospheric magnetic field their energy increases due to betatron acceleration. For a steep energy spectrum even a relatively weak enhancement of magnetic field leads to a considerable increase of fluxes. If depression is produced by the ring current, inside the current ring the magnetic field depression can be roughly estimated as $\Delta B = (2/3)|D_{st}|$. A similar depression of B may be produced by an enhanced plasma pressure p_m along a flux tube conjugate to the auroral oval. According to this mechanism, the position L_m of a belt of accelerated electrons corresponds to a region with maximal magnetic field depression $\Delta B_m \sim (5/3)\Delta B$. The statistical relationship between the flux maximum L_m and the Dst-index magnitude $|D_{st}| \sim L_m^{-4}$ is considered as a support of this conjecture (Tverskaya 1996). This relationship can be comprehended as a result of adiabatic acceleration, when a group of particles is transferred into a magnetic flux tube with a smaller specific volume $W \sim L^4$ (Tverskoy B.A. 1997). Thus, the problem of electron acceleration should be considered in coordination with the partial ring current and auroral oval dynamics (Antonova et al. 2009). In support of this view, it was found that during the storm maximum the westward electrojet moved to its lowest L-position at which a peak of the belt of relativistic electrons finally occurred (Tverskaya 1996; Tverskaya et al. 2005). Moreover, the peak of the symmetric ring current (pressure) was found to coincide with the peak of storm-injected belt of relativistic electrons (Tverskaya 2000). However, the above mechanism, relying on a substantial suppression of the magnetospheric magnetic field by the ring current, cannot interpret the occurrence of high electron fluxes during non-storm (|SYM-H| < 20 nT) events described above. Probably, during these events the energization of electrons took place due to activation of substorm activity and stimulation of ULF wave power by high solar wind streams.

The consideration of the above events has shown that there are at least several magnetospheric factors that are important for the magnitude of the electron response at geosynchronous orbit and inside it to space weather disturbances: extended substorm activity, solar wind speed, density, enhanced ULF power, and VLF chorus power. The ULF power increase commonly coincides with the growth of the VLF power. Therefore, it is not easy to separate these mechanisms by time of action. The solar wind disturbances stimulate ULF waves inside the magnetosphere and substorm activity. The energetic electrons injected during substorms excite VLF emissions, whereas the tens of keV electrons serve as seed particles for further acceleration. The magnetic storm is shown not to be a key factor for a prominent killer-electron response, but during storm the relativistic electron fluxes are higher than those during non-storm interval with a high solar wind speed. Besides ULF and VLF mechanisms, adiabatic betatron acceleration in the recovering magnetic field can produce an additional electron energization.

Conclusions

We have compared the relativistic electron fluxes during magnetic storms and non-storm time intervals. Some of the most powerful CME magnetic storms for the Arase satellite era have been considered: May 27–29, 2017, September 7–10, 2017, and August 25–28, 2018.

Belakhovsky *et al. Earth, Planets and Space*   (2023) 75:189

Page 15 of 17

During three events under consideration the relativistic electron fluxes during storm (with an average solar wind speed) are found to be greater than during non-storm intervals with a high solar wind speed. During magnetic storms, the flux intensity maximum shifts to lower L-shells compared to intervals without storms. The necessary condition for the increase of relativistic electron fluxes is the substorm intensification characterized by the growth of AE index. The examination of the event on May 27–30, 2017 has shown that a high solar wind speed is not always necessary condition for the appearance of the MeV electrons. Since the jump of the solar wind density generates ULF waves in the magnetosphere which can accelerate electrons.

The analysis shows that the growth of VLF and ULF wave activity occurs approximately at the same time, 1–3 days before the growth of the relativistic electrons, and coincides with the growth of substorm activity. We suppose that the ULF/VLF activity is responsible for the electron acceleration in the first phase, while the betatron mechanism due to recovering magnetic field gives an additional energy to electrons during the second phase, in absence of the high ULF/VLF activities.

Abbreviations

ULF	Ultra low frequency
VLF	Very low frequency
ORB	Outer radiation belt
MHD	Magnetohydrodynamics
FLR	Field-line resonance

Availability of data and materials
The Arase satellite data are available at the webpage ergsc.isee.nagoya-u.ac.jp, the GOES satellite data are available at the site cdaweb.gsfc.nasa.gov, the ULF index are available at the webpage ulf.gcras.ru, and the solar wind parameters from the OMNI database are taken from the webpage cdaweb.gsfc.nasa.gov.

Declarations

Ethics approval and consent to participate
Not applicable.

Consent for publication
Not applicable.

Competing interests
All coauthors have no competing interests.

Author details
[1]Polar Geophysical Institute, Apatity, Russia. [2]Institute of Physics of the Earth, Moscow, Russia. [3]Skobeltsyn Institute of Nuclear Physics, Lomonosov Moscow State University, Moscow, Russia. [4]Institute for Space-Earth Environmental Research, Nagoya University, Nagoya, Japan. [5]Kanazawa University, Kanazawa, Japan. [6]Tokyo University, Tokyo, Japan. [7]Japan Aerospace Exploration Agency, Tokyo, Japan. [8]Institute of Space and Astronautical Science, Tokyo, Japan. [9]Nagoya University, Nagoya, Japan. [10]Osaka University, Osaka, Japan.

References

Antonova EE (2006) Stability of the magnetospheric plasma pressure distribution and magnetospheric storms. Adv Space Res 38:1626–1630. https://doi.org/10.1016/j.asr.2005.05.005

Antonova EE, Stepanova MV (2015) The problem of the acceleration of electrons of the outer radiation belt and magnetospheric substorms. Earth Planet Space 67:148. https://doi.org/10.1186/s40623-015-0319-7

Antonova EE, Kirpichev IP, Stepanova MV, Orlova KG, Ovchinnikov IL (2009) Topology of the high latitude magnetosphere during large magnetic storms and the main mechanisms of relativistic electron acceleration. Adv Space Res 43(4):628–633. https://doi.org/10.1016/j.asr.2008.09.011

Antonova EE, Stepanova MV, Moya PS, Pinto VA, Vovchenko VV, Ovchinnikov IL, Sotnikov NV (2018) Processes in auroral oval and outer electron radiation belt. Earth Planet Space 70:127. https://doi.org/10.1186/s40623-018-0898-1

Baker DN, Daglis IA (2007) Radiation belts and ring current. In: Bothmer V, Daglis IA (eds) Space weather: physics and effects. Springer, Berlin, pp 173–202

Baker DN, Belian RD, Higbie PR, Hones EW Jr (1979) High energy magnetospheric protons and their dependence on geomagnetic and interplanetary conditions. J Geophys Res 84(A12):7138–7154. https://doi.org/10.1029/JA084iA12p07138

Belakhovsky VB, Pilipenko VA, Sakharov YA, Lorentzen DL, Samsonov SN (2017) Geomagnetic and ionospheric response to the interplanetary shock on January 24, 2012. Earth Planet Space 69(1):105. https://doi.org/10.1186/s40623-017-0696-1

Blake JB, Baker DN, Turner N, Ogilvie KW, Lepping RP (1997) Correlation of changes in the outer-zone relativistic-electron population with upstream solar wind and magnetic field measurements. Geophys Res Lett 24(8):927–929. https://doi.org/10.1029/97GL00859

Borovsky JE, Denton MH (2006) Differences between CME-driven storms and CIR-driven storms. J Geophys Res. 111:A07S08. https://doi.org/10.1029/2005JA011447

Boyd AJ, Turner DL, Reeves GD, Spence HE, Baker DN, Blak JB (2018) What causes radiation belt enhancements: a survey of the Van Allen Probes Era. Geophys Res Lett 45:5253–5259. https://doi.org/10.1029/2018GL077699

Capman NSS, Simms LE, Engebretson MJ, Clilverd MA, Rodger CJ, Reeves GD, Lessard MR, Gjerloev J (2019) Comparison of multiple and logistic regression analyses of relativistic electron flux enhancement at geosynchronous orbit following storms. J Geophys Res 124(12):10246–10256. https://doi.org/10.1029/2019JA027132

Elkington SR, Hudson MK, Chan AA (1999) Acceleration of relativistic electrons via drift-resonant interaction with toroidal-mode Pc-5 ULF oscillations. Geophys Res Lett 26:3273–3276. https://doi.org/10.1029/1999GL003659C

Foster JC, Erickson PJ, Omura Y, Baker DN, Kletzing CA, Claudepierre SG (2017) Van Allen Probes observations of prompt MeV radiation belt electron acceleration in nonlinear interactions with VLF chorus. J Geophys Res 122:324–339. https://doi.org/10.1002/2016JA023429

Hao YX, Zong Q-G, Zhou X-Z, Rankin R, Chen XR, Liu Y et al (2019) Global-scale ULF waves associated with SSC accelerate magnetospheric

ultrarelativistic electrons. J Geophys Res 124:1525–1538. https://doi.org/10.1029/2018JA026134

Higashio N, Takashima T, Shinohara I, Matsumoto H (2018) The extremely high-energy electron experiment (XEP) onboard the Arase (ERG) satellite. Earth Planet Space 70:134. https://doi.org/10.1186/s40623-018-0901-x

Hudson M, Jaynes A, Kress BT, Li Z, Patel M, Shen X-C, Wygant J (2017) Simulated prompt acceleration of multi-MeV electrons by the 17 March 2015 interplanetary shock. J Geophys Res 122:10036–10046. https://doi.org/10.1002/2017JA024445

Jaynes AN, Baker DN, Singer HJ, Rodriguez JV et al (2015) Source and seed populations for relativistic electrons: their roles in radiation belt changes. J Geophys Res 120:7240–7254. https://doi.org/10.1002/2015JA021234

Kanekal SG, Baker DN, Fennell JF, Jones A, Schiller Q, Richardson IG et al (2016) Prompt acceleration of magnetospheric electrons to ultrarelativistic energies by the 17 March 2015 interplanetary shock. J Geophys Res 121:7622–7635. https://doi.org/10.1002/2016JA022596

Kasahara S, Yokota S, Mitani T, Asamura K, Hirahara M, Shibano Y, Takashima T (2018a) Medium-energy particle experiments—electron analyzer (MEP-e) for the exploration of energization and radiation in geospace (ERG) mission. Earth Planet Space 70:69. https://doi.org/10.1186/s40623-018-0847-z

Kasahara Y, Kasaba Y, Kojima H, Yagitani S, Ishisaka K, Kumamoto A, Tsuchiya F, Ozaki M, Matsuda S, Imachi T, Miyoshi Y, Hikishima M, Katoh Y, Ota M, Shoji M, Matsuoka A, Shinohara I (2018b) The plasma wave experiment (PWE) on board the Arase (ERG) satellite. Earth Planet Space 70:86. https://doi.org/10.1186/s40623-018-0842-4

Katsavrias C, Daglis IA, Li W, Dimitrakoudis S, Georgiou M, Turner DL, Papadimitriou C (2015) Combined effects of concurrent Pc5 and chorus waves on relativistic electron dynamics. Ann Geophys 33:1173–1181. https://doi.org/10.5194/angeo-33-1173-2015

Kim H-J, Lyons L, Pinto V, Wang C-P, Kim K-C (2015) Revisit of relationship between geosynchronous relativistic electron enhancements and magnetic storms. Geophys Res Lett 42:6155–6161. https://doi.org/10.1002/2015GL065192

Kivelson MG, Pu ZY (1984) The Kelvin-Helmholtz instability on the magnetopause. Planet Space Sci 32(11):1335–1341. https://doi.org/10.1016/0032-0633(84)90077-1

Kozyra JU, Liemohn MW, Clauer CR, Ridley AJ, Thomsen MF, Borovsky JE, Roeder JL, Jordanova VK, Gonzalez WD (2002) Multistep Dst development and ring current composition changes during the 4–6 June 1991 magnetic storm. J Geophys Res 107(A8):1224. https://doi.org/10.1029/2001JA000023

Lazutin LL (2013) Injection of relativistic electrons into the internal magnetosphere during magnetic storms: connection with substorms. Geomag Aeron 53:716–732. https://doi.org/10.1134/S0016793213050113

Li X, Baker DN, Temerin M, Cayton TE, Reeves EGD, Christensen RA, Blake JB, Looper MD, Nakamura R, Kanekal SG (1997) Multisatellite observations of the outer zone electron variation during the November 3–4, 1993, magnetic storm. J Geophys Res 102(A7):14123–14140

Li W, Ni B, Thorne RM, Bortnik J, Green JC, Kletzing CA, Kurth WS, Hospodarsky GB (2013) Constructing the global distribution of chorus, wave intensity using measurements of electrons by the POES satellites and waves by the Van Allen Probes. Geophys Res Lett 40:4526–4532. https://doi.org/10.1002/grl.50920

Li L, Omura Y, Zhou X-Z, Zong Q-G, Rankin R, Yue C, Fu S-Y, Ren J (2023) Chorus wave generation modulated by field line resonance and mirror-mode ULF waves. J Geophys Res 128(2):e2022JA031127. https://doi.org/10.1029/2022JA031127

Liu WW, Rostoker G, Baker DN (1999) Internal acceleration of relativistic electrons by large-amplitude ULF pulsations. J Geophys Res 104:17391–17407. https://doi.org/10.1029/1999JA900168

Lyatsky W, Khazanov GV (2008) Effect of geomagnetic disturbances and solar wind density on relativistic electrons at geostationary orbit. J Geophys Res 113:A08224. https://doi.org/10.1029/2008JA013048

Matsuda S, Kasahara Y, Kojima H, Kasaba Y, Yagitani S, Ozaki M, Imachi T, Ishisaka K, Kumamoto A, Tsuchiya F, Ota M, Kurita S, Miyoshi Y, Hikishima M, Matsuoka A, Shinohara I (2018) Onboard software of plasma wave experiment aboard Arase: instrument management and signal processing of waveform capture/onboard frequency analyzer. Earth Planet Space 70:75 https://doi.org/10.1186/s40623-018-0838-0

Meredith NP, Horne RB, Illes RHA, Thorne RM, Heynderickx D, Anderson RR (2002) Outer zone relativistic electron acceleration associated with substorm-enhanced whistler mode chorus. J Geophys Res 107(A7):1144. https://doi.org/10.1029/2001JA900146

Miyoshi Y, Kataoka R (2005) Ring current ions and radiation belt electrons during geomagnetic storms driven by coronal mass ejections and corotating interaction regions. Geophys Res Lett 32:L21105. https://doi.org/10.1029/2005GL024590

Miyoshi Y, Kataoka R, Kasahara Y, Kumamoto A, Nagai T, Thomsen MF (2013) High-speed solar wind with southward interplanetary magnetic field causes relativistic electron flux enhancement of the outer radiation belt via enhanced condition of whistler waves. Geophys Res Lett 40:4520–4525. https://doi.org/10.1002/grl.50916

Miyoshi Y, Hori T, Shoji M, Teramoto M, Chang TF, Matsuda S, Kurita S, Segawa T, Umemura N, Keika K, Miyoshita Y, Tanaka Y, Nishitani N, Takashima T, Shinohara I (2018) The ERG Science Center. Earth Planet Space 70:96. https://doi.org/10.1186/s40623-018-0867-8

Moya PS, Pinto VA, Sibeck DG, Kanekal SG, Baker DN (2017) On the effect of geomagnetic storms on relativistic electrons in the outer radiation belt: Van Allen Probes observations. J Geophys Res 122(11):11100–11108. https://doi.org/10.1002/2017JA024735

Nopper RW, Hughes WJ, MacLennan CG, McPherron RL (1982) Impulse-excited pulsations during the July 29, 1977, event. J Geophys Res 87(A8):5911–5916. https://doi.org/10.1029/JA087iA08p05911

O'Brien TP, McPherron RL, Sornette D, Reeves GD, Friedel R, Singer HJ (2001) Which magnetic storms produce relativistic electrons at geosynchronous orbit? J Geophys Res 106(A8):15533–15544

O'Brien TP, Lorentzen KR, Mann IR, Meredith NP, Blake JB, Fennell JF, Looper MD, Milling DK, Anderson RR (2003) Energization of relativistic electrons in the presence of ULF power and MeV microbursts: evidence for dual ULF and VLF acceleration. J Geophys Res 108:1329. https://doi.org/10.1029/2002JA009784

Paulikas GA, Blake JB (1979) Effects of the solar wind on magnetospheric dynamics: energetic electrons at the synchronous orbit. In Quantitative modeling of magnetospheric processes, Geophys. Monogr. Ser., 21: 180–202, AGU, Washington, DC

Pilipenko V, Yagova N, Romanova N, Allen J (2006) Statistical relationships between satellite anomalies at geostationary orbit and high-energy particles. Adv Space Res 37:1192–1205. https://doi.org/10.1016/j.asr.2005.03.152

Pilipenko V, Kozyreva O, Belakhovsky V, Engebretson MJ, Samsonov S (2010) Generation of magnetic and particle Pc5 pulsations at the recovery phase of strong magnetic storms. Proc R Soc A. https://doi.org/10.1098/rspa.2010.0079

Pilipenko VA, Kozyreva OV, Engebretson MJ, Soloviev AA (2017) ULF wave power index for the space weather and geophysical applications: a review. Russ J Earth Sci 17:N2, ES1004. https://doi.org/10.2205/2017ES000597

Pinto VA, Kim H-J, Lyons LR, Bortnik J (2018) Interplanetary parameters leading to relativistic electron enhancement and persistent depletion events at geosynchronous orbit and potential for prediction. J Geophys Res 123:1134–1145. https://doi.org/10.1002/2017JA024902

Potapov AS, Tsegmed B, Ryzhakova LV (2012) Relationship between the fluxes of relativistic electrons at geosynchronous orbit and the level of ULF activity on the Earth's surface and in the solar wind during the 23rd solar activity cycle. Cosmic Res 50(2):124–140. https://doi.org/10.1134/S0010952512020086

Reeves GD, McAdams KL, Friedel RHW, O'Brien TP (2003) Acceleration and loss of relativistic electrons during geomagnetic storms. Geophys Res Lett 30(10):1529. https://doi.org/10.1029/2002GL016513

Reeves GD, Morley SK, Friedel RHW, Henderson MG, Cayton TE, Cunningham G, Blake JB, Christensen RA, Thomsen D (2011) On the relationship between relativistic electron flux and solar wind velocity: Paulikas and Blake revisited. J Geophys Res 116:A02213. https://doi.org/10.1029/2010JA015735

Reeves GD, Spence E, Henderson MG, Morley SK, Friedel RHW et al (2013) Electron acceleration in the heart of the Van Allen radiation belts. Science 341:991. https://doi.org/10.1126/science.1237743

Schiller Q, Li X, Blum L, Tu W, Turner DL, Blake JB (2014) A nonstorm time enhancement of relativistic electrons in the outer radiation belt. Geophys Res Lett 41:7–12. https://doi.org/10.1002/2013GL058485

Belakhovsky *et al. Earth, Planets and Space*   (2023) 75:189

Page 17 of 17

Shprits YY, Elkington SR, Meredith NP, Subbotin DA (2008a) Review of modeling of losses and sources of relativistic electrons in the outer radiation belt I: radial transport. J Atmos Solar-Terr Phys 70:1679–1693. https://doi.org/10.1016/j.jastp.2008.06.008

Shprits YY, Subbotin DA, Meredith NP, Elkington S (2008b) Review of modeling of losses and sources of relativistic electrons in the outer radiation belt II: local acceleration and loss. J Atmos Solar Terr Phys 70:1694–1713. https://doi.org/10.1016/j.jastp.2008.06.014

Simms LE, Engebretson MJ, Pilipenko V, Reeves GD, Clilverd M (2016) Empirical predictive models of daily relativistic electron flux at geostationary orbit: multiple regression analysis. J Geophys Res 121:3181–3197. https://doi.org/10.1002/2016JA022414

Simms LE, Engebretson MJ, Clilverd MA, Rodger CJ, Reeves GD (2018) Nonlinear and synergistic effects of ULF Pc5, VLF chorus, and EMIC waves on relativistic electron flux at geosynchronous orbit. J Geophys Res 123:4755–4766. https://doi.org/10.1029/2017JA025003

Simms LE, Engebretson MJ, Rodger CJ, Dimitrakoudis S, Mann IR, Chi PJ (2021) The combined influence of lower band chorus and ULF waves on radiation belt electron fluxes at individual L-shells. J Geophys Res 126:e2020JA028755. https://doi.org/10.1029/2020JA028755

Stepanova M, Pinto VA, Antonova EE (2021) Adiabatic and non-adiabatic evolution of relativistic electrons in the heart of the outer radiation belt during the 1 June 2013 geomagnetic storm. J Atmos Solar Terr Phys 212:105479. https://doi.org/10.1016/j.jastp.2020.105479

Summers D, Thorne RM, Xiaio F (1998) Relativistic theory of wave-particle resonant diffusion with application to electron acceleration in the magnetosphere. J Geophys Res 103(20):487

Takahashi N, Seki K, Fok M-C, Zheng Y, Miyoshi Y, Kasahara S et al (2021) Relative contribution of ULF waves and whistler-mode chorus to the radiation belt variation during the May 2017 storm. J Geophys Res 126:e2020JA028972. https://doi.org/10.1029/2020JA028972

Thorne RM, Li W, Ni B, Ma Q, Bortnik J, Chen L, Baker DN et al (2013) Rapid local acceleration of relativistic radiation belt electrons by magnetospheric chorus. Nature 504:411–414. https://doi.org/10.1038/nature12889

Tsurutani BT, Smith EJ (1977) Two types of magnetospheric ELF chorus and their substorm dependencies. J Geophys Res 82:5112. https://doi.org/10.1029/JA082i032p05112

Tverskaya LV (1996) Dynamics of energetic electrons in the radiation belts. Geophys Monogr. 97. AGU. P. 183–186

Tverskaya LV (2000) Diagnosing the storm-time ring current and other magnetospheric plasma domains using relativistic electron data. Adv Space Res 25(12):2315–2318. https://doi.org/10.1016/S0273-1177(99)00515-3

Tverskaya LV, Ivanova TA, Pavlov NN, Ya. Reizman S, Rubinstein IA, Sosnovets EN, Veden'kin NN (2005) Storm-time formation of a relativistic electron belt and some relevant phenomena in other magnetosphere plasma domains. Adv Space Res 36:2392–2400. https://doi.org/10.1016/j.asr.2003.09.071

Tverskoy BA (1997) Formation mechanism of the ring current structure of magnetic storms. Geomag Aeron 37(5):29–34 (**in Russian**)

Ukhorskiy AY, Sitnov MI, Takahashi K, Anderson BJ (2009) Radial transport of radiation belt electrons due to stormtime Pc5 waves. Ann Geophys 27:2173–2181. https://doi.org/10.5194/angeo-27-2173-2009

Publisher's Note